

Article

# Game-Based Hierarchical Cooperative Control for Electric Vehicle Lateral Stability via Active Four-Wheel Steering and Direct Yaw-Moment Control

Lin Zhao <sup>1</sup>, Shaobo Lu <sup>1,2,\*</sup> and Bohan Zhang <sup>1</sup> <sup>1</sup> School of Automotive Engineering, Chongqing University, Chongqing 400040, China<sup>2</sup> State Key Laboratory of Mechanical Transmission, Chongqing University, Chongqing 400040, China

\* Correspondence: lsba@163.com; Tel.: +86-181-008-69754

Received: 10 July 2019; Accepted: 27 August 2019; Published: 29 August 2019



**Abstract:** A Stackelberg game-based cooperative control strategy is proposed for enhancing the lateral stability of a four-wheel independently driving electric vehicle (FWID-EV). An upper-lower double-layer hierarchical control structure is adopted for the design of a stability control strategy. The leader-follower-based Stackelberg game theory (SGT) is introduced to model the interaction between two unequal active chassis control subsystems in the upper layer. In this model, the direct yaw-moment control (DYC) and the active four-wheel steering (AFWS) are treated as the leader and the follower, respectively, based on their natural characteristics. Then, in order to guarantee the efficiency and convergence of the proposed control strategy, a sequential quadratic programming (SQP) algorithm is employed to solve the task allocation problem among the distributed actuators in the lower layer. Also, a double-mode adaptive weight (DMAW)-adjusting mechanism is designed, considering the negative effect of DYC. The results of cosimulation with *CarSim* and *Matlab/Simulink* demonstrate that the proposed control strategy can effectively improve the lateral stability by properly coordinating the actions of AFWS and DYC.

**Keywords:** active four-wheel steering; direct yaw-moment control; lateral stability control; Stackelberg game theory; sequential quadratic programming

## 1. Introduction

Due to increasing demand for a low-carbon society, fully electric vehicles (EV) have drawn much attention in the automotive field [1,2]. In particular, research into four-wheel independently driving electric vehicles (FWID-EV) equipped with in-wheel motors to drive each wheel has become more intense in recent years because of the possibility of realizing fast response, high accuracy, and flexible maneuverability [3]. However, the coordination among the distributed in-wheel motors and other actuators for vehicle stability control would be one of the most challenging problems that designers will have to confront.

Active steering like AFS and driving/braking-based yaw moment control systems like direct yaw-moment control (DYC) are major parts of active stability control systems, which play important roles in improving a vehicle's dynamic performance [4]. DYC stabilizes the vehicle by generating additional yaw moment when it deviates from the desired states [5]. Due to the strongly coupled characteristics of a vehicle chassis, these subsystems would produce mutual influences on each other when working simultaneously under adverse situations [6]. As a result, the coordinated control of multiple subsystems of a chassis for improving vehicle performance has become a hot research topic in recent years [7,8].

However, most of this research generally only gives the invariant control authority to the subsystems (i.e., AFS and DYC). Actually, the role of AFS decreases gradually as the lateral tire force

approaches the adhesion limit [9], whereas DYC could play an effective role under these extreme conditions. This phenomenon reflects the variable control effects of AFS and DYC under changing vehicle states, and some research may not sufficiently consider the dynamic characteristics of the vehicle subsystems. Game theory is an effective method for dealing with the interaction of multiple agents, which provides a system control framework for this kind of cooperative control problem [10]. Since the AFS and DYC-based stability controller generally operate in an interactive manner as the vehicle travels ahead in a road tracking scenario, dynamic game theory should be applied.

Dynamic game theory is an optimal approach based on the decision theory and the rules of dynamic game, as defined by Cruz [11] and Basar [12]. There exist three core principles in the dynamic game theory [13]: (1) Each player's attitude towards his own as well as others' interests. (2) Each player's strategy adopted for pursuing their goal. (3) Each player's knowledge received about the state of the system during the game process. Based on these principles, different kinds of game rules are formed, such as for a noncooperative game and a cooperative game. (Due to limited space, for more details about game theory we refer readers to [13] and [14].) Assume that each subsystem aims to achieve individual rationality and to maximize the vehicle stability in its own way. Thus, this work mainly focuses on noncooperative game theory.

Noncooperative game theory has been widely studied to solve problems involving multiple individuals where their welfare is interactional [15]. It is an effective approach to address the problem of control authority allocation for multiple players [12]. Tamaddoni et al. [16,17] designed a vehicle lateral stability controller using differential game theory, in which the human driver and DYC were defined as two players with different control objects. Simulation results demonstrated that the vehicle's lateral stability and path tracking ability were greatly improved by the cooperation of the two players. Na et al. [18,19] used dynamic game theory to model the shared steering control between a human driver and AFS in feedback and open-loop modes, respectively, which is a successful early application of game theory in the field of human-machine interaction. Zhang et al. [20] indicated that active four-wheel steering (AFWS) could improve the maneuverability and stability of a vehicle better than AFS. Considering the good properties of game theory in solving multiple players' control problems and AFWS's better performance in vehicle dynamic control, dynamic game theory is used to realize the interactive control between AFWS and DYC in this paper. In particular, the open-loop Stackelberg game theory (SGT) is utilized to derive the cooperative control strategies between AFWS and DYC.

The Stackelberg equilibrium is a strategy set that can maximize each player's welfare, in which the players are divided into leader and follower. The leader has priority in making decisions, and knows the cost function mapping of the follower, while the follower does not know the cost function mapping of the leader [11]. However, the follower knows the decisions of the leader and the follower's control strategies are restricted by the leader's decisions [21]. In addition, the leader has the option to declare his/her strategy in advance, and then the follower formulates strategies by obeying the leader's decision. Finally, the strategies of the leader and follower together constitute the Stackelberg game result.

Due to the saturation of cornering forces, the performance of AFWS will be limited in some extreme conditions [22]. However, DYC could play an effective role in stabilizing the vehicle by differential driving/braking in this condition. Thus, the control authority of DYC is much larger than that of AFWS, especially in a nonlinear area. When they work simultaneously in this area, DYC behaves in a similar way to the leader and AFWS has similar properties to the follower. Therefore, in this study, DYC will function as the leader and AFWS as the follower in the Stackelberg game.

This paper focuses on the cooperation between AFWS and DYC to further improve the lateral stability of FWID-EV under extreme conditions. The main contributions of this study are threefold: First, inspired by [21], a leader-follower-based interactive control strategy between AFWS and DYC is proposed to deal with their unequal control authority based on dynamic game theory. Different from [21], this work mainly focuses on machine-machine cooperative control to properly determine the variable control authority between the two subsystems. Second, the tire forces the control allocation problem to the lower-level controller, which is tailored to a series of highly efficient quadratic

programming subproblems by the sequential quadratic programming (SQP) method. Finally, a novel variable weight-regulating mechanism is proposed based on the phase portraits of vehicle states to attenuate the difficulties of the proposed control strategy by considering the danger level of the vehicle.

The rest of the paper is organized as follows. Section 2 introduces the overall control scheme and the vehicle control model. Section 3 presents the process of upper-level controller designing, which includes the application of a Stackelberg game framework to the interactive controller between AFWS and DYC. Section 4 introduces the driving/braking torque distribution in the lower-level controller. The simulation results are presented in Sections 5 and 6 gives our conclusions.

## 2. Control Structure and Control-Oriented Model

### 2.1. Overall Control Strategy

The overall hierarchical control strategy used to realize the cooperative control of AFWS and DYC is presented in Figure 1. It includes two layers: an upper-level controller and a lower-level controller.

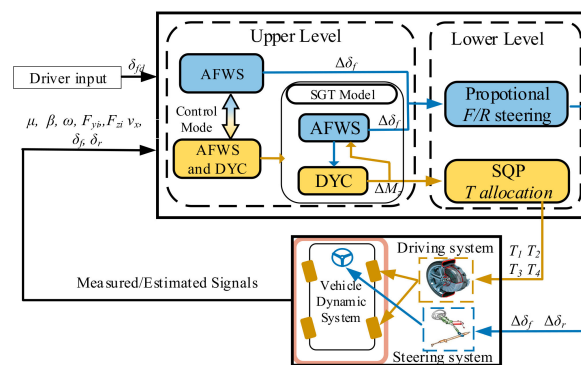


Figure 1. Overall hierarchical control strategy.

The upper-level controller works with a double-mode adaptive weight (DMAW)-adjusting mechanism to derive the front wheel steering angle and additional yaw moment by linking the AFWS and DYC. In the weight-adjusting mechanism, a single or hybrid control mode will be determined based on the detected effective working region. For the hybrid control mode, the cooperative control of AFWS and DYC is achieved based on the Stackelberg game theory.

In the lower-level controller, the virtual additional yaw moment will be transformed into the four wheels' driving/braking torque by the nonlinear optimization method. Also, the additional rear wheel steering angle of AFWS will be determined by a special principle of four-wheel steering.

### 2.2. Control-Oriented Model

As presented in Figure 2, a linearized two-DoF vehicle model is used to design the control system. The main purpose of the control system is to let the vehicle follow the desired states. We assume that the steering characteristics of the left and right tires are the same. The lateral and yaw motion equations can be expressed as follows [23]:

$$\begin{cases} mv_x(\dot{\beta} + \omega) = F_{yf} + F_{yr} \\ I_z \dot{\omega} = aF_{yf} - bF_{yr} + \Delta M_z \end{cases} \quad (1)$$

with

$$\begin{cases} F_{yf} = k_f \alpha_f = k_f (\delta_{fd} + \Delta \delta_f - \beta - a\omega/v_x) \\ F_{yr} = k_r \alpha_r = k_r (\delta_{rd} + \Delta \delta_r - \beta + b\omega/v_x) \end{cases} \quad (2)$$

where  $\beta$  and  $\omega$  are the sideslip angle and yaw rate of the vehicle, respectively.  $\delta_{fd}$  is the front wheel steering angle generated by the driver,  $\delta_{rd}$  is the rear wheel steering angle.  $\Delta \delta_f$  and  $\Delta \delta_r$  are the

additional front and rear wheel steering angles, respectively, and  $\delta_f = \delta_{fd} + \Delta\delta_f$  and  $\delta_r = \delta_{rd} + \Delta\delta_r$ , which are the total front and rear wheel steering angles, respectively.  $F_{yf}$  and  $F_{yr}$  are the lateral tire forces of the front wheels and rear wheels, respectively.  $\Delta M_z$  is the additional yaw moment that is produced by the DYC system.  $m$  is the vehicle mass,  $v_x$  is the longitudinal velocity, and  $a$  and  $b$  are the distance from the vehicle's c.g. (center of gravity) to the front and rear axles, respectively.  $I_z$  is the moment of inertia.  $k_f$  and  $k_r$  are the positive cornering stiffness of the front and rear axles, respectively. Therefore, the canonical state equation of the linear single track dynamic model can be derived as follows:

$$\dot{x}_{ac} = A_{ac}x_{ac} + B_{11}\Delta\delta_f + B_{12}\Delta\delta_r + B_2\Delta M_z + E_{ac1}\delta_{fd} + E_{ac2}\delta_{rd}, \quad (3)$$

with

$$\begin{aligned} x_{ac} &= \begin{bmatrix} \beta \\ \omega \end{bmatrix}, A_{ac} = \begin{bmatrix} -\frac{(k_f+k_r)}{mv_x} & \frac{-ak_f+bk_r}{mv_x^2} - 1 \\ \frac{-ak_f+bk_r}{I_z} & \frac{-a^2k_f-b^2k_r}{I_z v_x} \end{bmatrix}, B_{11} = \begin{bmatrix} \frac{k_f}{mv_x} \\ \frac{ak_f}{I_z} \end{bmatrix} \\ B_{12} &= \begin{bmatrix} \frac{k_r}{mv_x} \\ \frac{bk_r}{I_z} \end{bmatrix}, B_2 = \begin{bmatrix} 0 \\ \frac{1}{I_z} \end{bmatrix}, E_{ac1} = \begin{bmatrix} \frac{k_f}{mv_x} \\ \frac{ak_f}{I_z} \end{bmatrix}, E_{ac2} = \begin{bmatrix} \frac{k_r}{mv_x} \\ \frac{bk_r}{I_z} \end{bmatrix}. \end{aligned} \quad (4)$$

For improving the vehicle's stability under different velocity, the proportional four-wheel steering principle proposed by Sano et al. [24] is adopted:

$$\iota = \frac{\delta_r}{\delta_f} = \frac{-b + mav_x^2/[k_r(a+b)]}{a + mbv_x^2/[k_f(a+b)]}. \quad (5)$$

Then, the state equation can be simplified as follows:

$$\dot{x}_{ac} = A_{ac}x_{ac} + B_1\Delta\delta_f + B_2\Delta M_z + E_{ac}\delta_{fd}, \quad (6)$$

with

$$\begin{cases} B_1 = B_{11} + \iota \cdot B_{12} \\ E_{ac} = E_{ac1} + \iota \cdot E_{ac2} \end{cases} \quad (7)$$

where  $x_{ac} = [\beta, \omega]^T$  is the state variable. The desired responses of the yaw rate and sideslip angle can be obtained based on the steering angle of driver input, which can be modeled as the first-order response of front wheel steering input and described as follows [25,26]:

$$\begin{cases} \omega_d = \Xi_\omega / (1 + \tau_\omega s) \cdot \delta_{fd} \\ \beta_d = \Xi_\beta / (1 + \tau_\beta s) \cdot \delta_{fd} \end{cases} \quad (8)$$

with

$$\begin{cases} \Xi_\omega = \frac{v_x}{(a+b) + mv_x^2(bk_r - ak_f)/[k_f k_r(a+b)]} \\ \Xi_\beta = \frac{b - amv_x^2/[k_r(a+b)]}{(a+b) + mv_x^2(bk_r - ak_f)/[k_f k_r(a+b)]} \end{cases} \quad (9)$$

where the time constant is defined as follows [25]:

$$\tau_\omega = \tau_\beta = \frac{I_z v_x}{ak_f(a+b) + bmv_x^2}. \quad (10)$$

Meanwhile, the nominal values of vehicle states are restricted by the tire-road adhesion coefficient  $\mu$ , which can be expressed as follows [23]:

$$\begin{cases} |\omega_d| \leq \frac{\mu g}{v_x} \\ |\beta_d| \leq \tan^{-1}(0.02\mu g) \end{cases} \quad (11)$$

Based on the desired state responses in Equation (8), the error state (Equation) can be derived according to the work of Yang et al. [25], and is constructed as follows:

$$\Delta \dot{x} = A_{ac} \Delta x + B_1 \Delta \delta_f + B_2 \Delta M_z, \tag{12}$$

with

$$\Delta x = x_{ac} - x_d = \begin{bmatrix} \beta - \beta_d \\ \omega - \omega_d \end{bmatrix}, \tag{13}$$

$$x_d = \begin{bmatrix} \beta_d & \omega_d \end{bmatrix}^T$$

where  $x_d$  represents the desired state responses of vehicle.

For constructing the discrete-time Stackelberg game, the continuous error state equation (Equation (12)) is translated into a discrete form with the sample time  $T_s$  as 0.01 s.

$$\Delta x(k+1) = A_{ad} \Delta x(k) + B_{1d} \Delta \delta_f(k) + B_{2d} \Delta M_z(k), \tag{14}$$

where

$$A_{ad} = e^{A_{ac} T_s}, B_{1d} = B_1 \int_0^{T_s} e^{A_{ac} t} dt, B_{2d} = B_2 \int_0^{T_s} e^{A_{ac} t} dt. \tag{15}$$

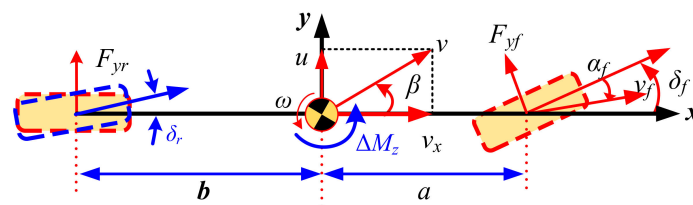


Figure 2. Two-DoF control model.

### 3. Upper-Level Controller

#### 3.1. Division of Control Modes

In order to clearly judge the safety states of the vehicle, a  $\beta$ - $\omega$  phase portrait analysis method is adopted, which is an important way to judge the safety of the vehicle [27]. In order to clearly express the working states of the vehicle and improve its performance in different states, the working region is divided into four parts as shown in Figure 3—namely, a safety region in part I, a defective safety region in part II, an unstable region in part III, and a dangerous region in part IV. The division of the four working regions and boundaries is based on the dynamic characteristics of the vehicle [23] and calibrated by simulation tests in specific conditions [28]. To visually express the vehicle states in different working regions, the plotting scale is adjusted to make it an ideal circle.

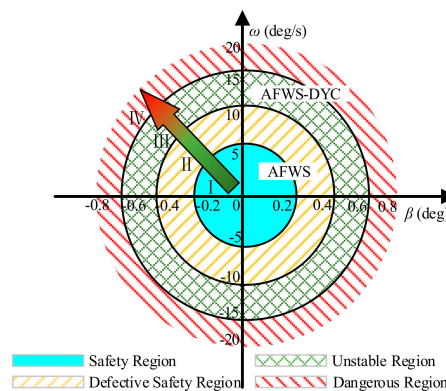


Figure 3. Working region of AFWS and DYC.

Considering the vehicle’s lateral stability and the driver’s feeling of control using the upper-level controller, two control modes are defined based on the working region in Figure 3: (1) Single AFWS control and (2) hybrid AFWS-DYC control.

As presented in Figure 3, the two-dimensional working region control mode with respect to  $\beta$ - $\omega$  phase plane is defined. When the sideslip angle  $\beta$  and the yaw rate  $\omega$  are small and stay in regions I and II, the DYC would be closed and only AFWS works. This is because the DYC would impose additional yaw moment by differential driving/braking, which can lead to evidently uncomfortable yaw motion on humans due to the sudden change in the vehicle’s longitudinal dynamics. Compared with DYC, the action of AFWS can almost be neglected due to its small range. In addition, the application of steer-by-wire technology can also remove the overlapped steering effect that can make drivers uncomfortable [29].

When  $\beta$  and  $\omega$  become larger and enter region III/IV, the hybrid AFWS-DYC control mode will work to ensure the vehicle’s lateral stability and safety. This is because when the sideslip angle and yaw rate become larger, AFWS could not provide sufficient lateral tire force to keep the vehicle stable [23], but DYC can play a central role in stabilizing the vehicle by differential driving/braking in these regions.

Sideslip angle and yaw rate are two important parameters that can represent the lateral stability of a vehicle [27]. Therefore, a coefficient weighting method [28] is used to construct the dangerous factor (DF), which can denote the danger level of the vehicle and is defined based on the weighting of the two parameters  $\beta, \omega$ . DF can be represented as follows:

$$DF = \sqrt{(p\beta)^2 + (q\omega)^2} \tag{16}$$

where  $p$  and  $q$  are the weight. Assuming that the state variables  $\beta$  and  $\omega$  can be estimated or measured based on an advanced sensing method such as a global positioning system (GPS), inertial measurement unit (IMU), or gyroscope [30]. For DF to equally reflect the features of  $\beta$  and  $\omega$ , their weights are set as  $p = 25, q = 1$  based on the scale of  $\beta, \omega$  presented in Figure 3.

### 3.2. Stackelberg Game-Based Coordinated Control Strategy

Figure 4 shows the Stackelberg game interactive control paradigm between DYC and AFWS. It is constructed following the ideas presented in [14]. The Stackelberg equilibrium strategy is a leader-follower control mode, in which the DYC functions as the leader and has the pioneering authority to make decisions by considering the AFWS’s (follower’s) responses [31], whereas the follower makes decisions by simply responding to the DYC’s decision.

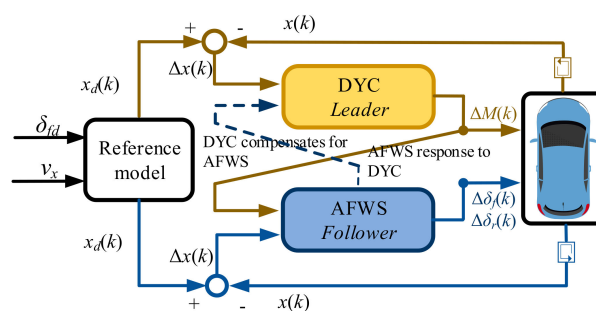


Figure 4. DYC and AFWS Stackelberg game control paradigm.

In this section, a linear quadratic differential game is used to construct the Stackelberg game control model. The process includes two main steps: (1) Construction of cost functions; (2) application of Stackelberg game strategy to the controller.

**Remark 1.** To clearly show the game process, a two-dimensional evolution diagram is constructed based on the ideas of [21]. As shown in Figure 5, the discrete control system develops as the game proceeds.  $\Delta x_0(0)$  represents the initial state error and players begin the game from stage 0 to  $N$ . The 0 in  $\Delta x_0(0)$  represents the time step and the game stage, where 0 in parentheses denotes the time step and the 0 in a subscript denotes the stage of the game. In game stage 0, after the two players' game actions are applied to the control system, the game stage then moves to stage 1, namely,  $\Delta x_1(0)$ . After  $N$ -stage similar game process, the game stage reaches  $\Delta x_N(0)$  and the time step starts moving to the next time step,  $\Delta x(1)$  or  $\Delta x_0(1)$ . At each time step, the game would proceed  $N$ -stage game and then move to the next time step. In conclusion, at any time step  $n$ , the initial error state is  $\Delta x_0(n)$ , which is the same as  $\Delta x(n)$ , and the middle game stage can be represented as  $\Delta x_i(n)$ , where  $i = 1, 2, 3 \dots N$ . In the game process of each time step  $n$ , each player only knows the initial state information  $\Delta x_0(n)$  in the open-loop Stackelberg game pattern.

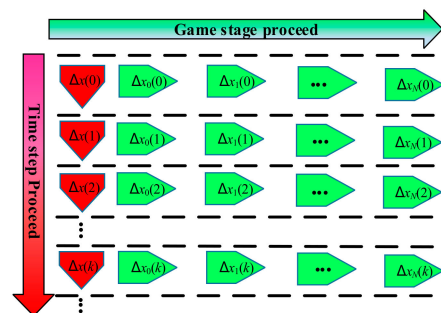


Figure 5. The detailed process of game optimization.

### 3.2.1. Construction of Cost Function

In the AFWS-DYC cooperative lateral stability control problem, DYC tries to reduce the state error  $\Delta x_i(k)$  by considering the amount of control variable  $\Delta M_{zi}(k)$ . The control object of DYC is constructed based on this characteristic. As shown in [32], the cost function of DYC can be represented as follows:

$$\begin{cases} J_1(k) = \frac{1}{2} \Delta x_N^T(k) S_1 \Delta x_N(k) + \sum_{i=0}^{N-1} [G_i^1(k)] \\ G_i^1(k) = \frac{1}{2} [\Delta x_i^T(k) Q_1 \Delta x_i(k) + \Delta M_{zi}^T(k) R_1 \Delta M_{zi}(k)] \end{cases}, \quad (17)$$

where  $\Delta x_i(k)$  denotes the state error at  $i$ th stage game at time step  $k$ ,  $\Delta x_N(k)$  represents the terminal error state, and  $\Delta M_{zi}(k)$  is the additional yaw moment.  $Q_1$  is the state-error weight matrix, which is the same as the terminal state error weight  $S_1$ , and  $R_1$  is the weight matrix of DYC.

The cost function of AFWS is constructed in the same way, with the aim of reducing the error of state variables and additional steering angle. The corresponding cost function can be expressed as follows:

$$\begin{cases} J_2(k) = \frac{1}{2} \Delta x_N^T(k) S_2 \Delta x_N(k) + \sum_{i=0}^{N-1} G_i^2(k) \\ G_i^2(k) = \frac{1}{2} [\Delta x_i^T(k) Q_2 \Delta x_i(k) + \Delta \delta_{fi}^T(k) R_2 \Delta \delta_{fi}(k)] \end{cases}, \quad (18)$$

where  $\Delta \delta_{fi}$  is the corresponding additional front wheel steering angle.  $Q_2$  is the state-error weight matrix, which is the same as the terminal state error weight matrix  $S_2$ , and  $R_2$  is the weight matrix of AFWS. The standard form of  $Q_i$  ( $i = 1, 2$ ) and  $R_i$  ( $i = 1, 2$ ) are expressed as follows:

$$\begin{cases} Q_i = \text{diag} [ Q_\beta \quad Q_\omega ] \\ R_1 = R_{Mz}, R_2 = R_\delta \end{cases}, \quad (19)$$

where  $Q_\beta$ ,  $Q_\omega$ ,  $R_\delta$ , and  $R_{Mz}$  are the weight of  $\beta$ ,  $\omega$ ,  $\delta$ , and  $M_z$ , respectively.

**Remark 2.** As shown in Figure 3, there are two control modes in the upper-level controller: single AFWS control and hybrid AFWS-DYC control. The switching of the control modes is achieved by adjusting the weight coefficient of the inputs. In single AFWS control mode, only the steering system works to ensure the stability of the vehicle. The weight coefficient for AFWS control mode is defined as follows:

$$[R_{\delta}, R_{Mz}] = [50, \text{Inf}], \quad (20)$$

where *Inf* represents infinity, and restricts the output of DYC to 0 in single AFWS mode. When the hybrid AFWS-DYC control mode is adopted, both DYC and AFWS work together to ensure the stability of the vehicle. For reducing the influence of the DYC on a human driver in this hybrid mode, an adaptive weight-adjusting mechanism (AVAW) is designed. As the DF decreases, the control authority of DYC would also decrease because the AFWS could provide more lateral tire force for stabilizing the vehicle. When the control authority of DYC is decreased, less additional yaw moment will be added to the vehicle body and hence the discomfort of the human driver will be mitigated. The adaptive weight is defined as follows:

$$[R_{\delta}, R_{Mz}] = [100 - 0.005\sigma, \sigma], \quad (21)$$

with

$$\begin{cases} \sigma = \min(10,000, v) \\ v = 60,000/DF \end{cases} . \quad (22)$$

It is clear that  $\sigma$  increases as the value of the dangerous factor (DF) decreases.

### 3.2.2. Stackelberg Game-Based Controller

The information pattern of Stackelberg game strategy is assumed to be open-loop at each step. It indicates that the controller can only get the initial states of each step and then move to the next step after  $N$  stages game. As in the analysis process that presented in [33], the optimal game response of the follower ( $\Delta\delta_f$ ) should be determined first and the optimal problem can be constructed as follows:

$$\begin{aligned} & \min_{\Delta\delta_f} J_2(k) \\ \text{s.t.} & \begin{cases} f(k) = A_d \Delta x_i(k) + B_{1d} \Delta\delta_{fi}(k) + B_{2d} \Delta M_{zi}(k). \\ i = 0, 1, \dots, N-1. \end{cases} \end{aligned} \quad (23)$$

where the constraint in Equation (23) is the equation of game progression at time step  $k$ ; it has the same form as the error state in Equation (14). This is a standard optimal problem and the Lagrange multiplier method is used to solve it [12,21]. The augmented cost function of the follower is constructed as follows:

$$H_2(k) = \frac{1}{2} \Delta x_N^T(k) S_2 \Delta x_N(k) + \sum_{i=0}^{N-1} [G_i^2(k)] + \sum_{i=0}^{N-1} \{ \eta_{i+1}^T(k) f(k) \}, \quad (24)$$

where  $\eta_{i+1}(k)$  is the Lagrange multiplier at the corresponding game stage at time step  $k$ . The functions of  $f(k)$  and  $G_{i2}(k)$  have been defined in Equations (18) and (23), respectively.

**Lemma 1.** Basar et al. [12]) For ensuring the optimal response of the leader in Stackelberg game optimal control strategy and getting the minimum augmented cost function in Equation (24), the follower's control vector  $\Delta\delta_f(k)$  and Lagrange multiplier  $\eta_i(k)$  should satisfy the following relations:

$$\left\{ \begin{array}{l} (a). \eta_i(k) = \frac{\partial f(k)^T}{\partial \Delta x_i(k)} \left[ \eta_{i+1}(k) + \left( \frac{\partial G_i^2(k)}{\partial \Delta x_{i+1}(k)} \right)^T \right] + \left[ \frac{\partial G_i^2(k)}{\partial \Delta x_i(k)} \right]^T \\ \quad i = 0, 1, \dots, N-1 \\ \eta_N(k) = \partial \left( \frac{1}{2} \Delta x_N^T(k) S_2 \Delta x_N(k) \right) / \partial \Delta x_N, i = N \\ (b). \frac{\partial H_2(k)}{\partial \Delta \delta_{f_i}(k)} = 0, i = 0, 1, \dots, N-1 \end{array} \right. \quad (25)$$

By solving Equation (25), the necessary conditions that minimizing the augment function of Equation (24) are determined as follows:

$$\left\{ \begin{array}{l} (a). \eta_i(k) = A_d^T \eta_{i+1}(k) + Q_2 \Delta x_i(k), i = 0, 1, \dots, N-1. \\ \eta_N(k) = S_2 \Delta x_N(k), i = N \\ (b). R_2 \Delta \delta_{f_i}(k) + \eta_{i+1}^T(k) B_{1d} = 0, i = 0, 1, \dots, N-1 \end{array} \right. \quad (26)$$

Similarly, following the theory of Basar and Tamer [12], the game optimal control problem of leader (DYC) can be constructed in the following form:

$$\left\{ \begin{array}{l} \min_{\Delta M_z} J_1(k) \\ (a). f(k) = A_d \Delta x_i(k) + B_{1d} \Delta \delta_{f_i}(k) + B_{2d} \Delta M_{z_i}(k). \\ \quad i = 0, 1, \dots, N-1. \\ (b). Eq. (22a) \\ (c). Eq. (22b) \end{array} \right. \quad (27)$$

For realizing the Stackelberg game control mode, the leader (DYC) considers the action of the follower (AFWS) when making decisions, as shown in Figure 4. The necessary conditions of follower's (AFWS) optimal problem, Equation (27a) and (27b), are set as the constraints in leader's (DYC) optimal problem. Like Equation (24), the Lagrange multiplier method is also used to solve the optimization problem in Equation (27), and the augmented cost function of the leader is constructed as follows:

$$\begin{aligned} H_1(k) = & \frac{1}{2} \Delta x_N^T(k) S_1 \Delta x_N(k) + \sum_{i=0}^{N-1} [G_i^1(k)] + \sum_{i=0}^{N-1} \{ \gamma_i^T(k) f(k) \} \\ & + \sum_{i=0}^{N-1} \{ \kappa_i^T(k) [Q_2 \Delta x_i(k) + A_d^T \eta_{i+1}(k) - \eta_i(k)] \} \\ & + \sum_{i=0}^{N-1} \{ \varepsilon_i^T(k) [R_2 \Delta \delta_{f_i}(k) + \eta_{i+1}^T(k) B_{1d}] \} \end{aligned} \quad (28)$$

where  $\gamma_i(k)$ ,  $\kappa_i(k)$ , and  $\varepsilon_i(k)$  are the Lagrange multipliers of the corresponding constraint equations in Equation (28) at time step  $k$  with  $i = 0, 1, \dots, N-1$ .

**Lemma 2.** (Basar et al. [12]) For getting the minimum value of the augmented cost function in Equation (28), the Lagrange multipliers  $\gamma_i(k)$ ,  $\kappa_i(k)$ ,  $\varepsilon_i(k)$  and control vectors  $\Delta \delta_f(k)$ ,  $\Delta M_z(k)$  satisfy the following relations:

$$\left\{ \begin{array}{l} (a). \frac{\partial H_1(k)}{\partial \Delta \delta_{f_i}(k)} = 0, i = 0, 1, 2, \dots, N-1 \\ (b). \frac{\partial H_1(k)}{\partial \Delta M_{z_i}(k)} = 0, i = 0, 1, 2, \dots, N-1 \\ (c). \gamma_{i-1}^T(k) = \frac{\partial H_1(k)}{\partial \Delta x_i(k)}, i = 0, 1, 2, \dots, N-1 \\ \quad \gamma_{N-1}^T(k) = \frac{\partial H_1(k)}{\partial \Delta x_N(k)}, i = N \\ (d). \kappa_{i+1}^T(k) = \frac{\partial H_1(k)}{\partial \eta_{i+1}(k)}, i = 0, 1, 2, \dots, N-1 \\ \quad \kappa_0^T(k) = 0 \end{array} \right. \quad (29)$$

By solving Equation (29), the necessary conditions for minimizing the augment function are determined as follows:

$$\begin{cases} (a). \gamma_i^T(k)B_{1d} + \varepsilon_i^T(k)R_2 = 0, i = 0, 1, 2, \dots, N - 1 \\ (b). \gamma_i^T(k)B_{2d} + R_1\Delta M_{zi}(k) = 0, i = 0, 1, 2, \dots, N - 1 \\ (c). \gamma_{i-1}^T(k) = Q_1\Delta x_i(k) + \gamma_i^T(k)A_d + \kappa_i^T(k)Q_2, \\ \quad \gamma_{N-1}^T(k) = S_1\Delta x_N(k), i = 0, 1, 2, \dots, N - 1 \\ (d). \kappa_{i+1}^T(k) = \kappa_i^T(k)A_d^T + \varepsilon_i^T(k)B_{1d}^T, \kappa_0^T = 0 \\ \quad i = 0, 1, 2, \dots, N - 1 \end{cases} \quad (30)$$

Equations (26) and (30) constitute the necessary conditions for solving the open-loop Stackelberg control problem, which includes six equations and six variables, so it is a solvable equation set and the solutions of these equations are the control strategies of the leader and follower (DYC and AFWS).

**Lemma 3.** (Hungerländer and Neck [33]) Equations (26) and (30) constitute a two-point boundary value (TPBV) problem; however, the variables of it are interwoven, so it is difficult to solve. To deal with this problem, Hungerländer [33] designed two supplementary equations:

$$\begin{cases} \eta_i(k) = (M_i^x(k) - Q_2)\Delta x_i(k) + M_i^\kappa(k)\kappa_i(k) + m_i(k) \\ \gamma_i(k) = (L_i^x(k) - Q_1)\Delta x_i(k) + L_i^\kappa(k)\kappa_i(k) + l_i(k) \end{cases} \quad (31)$$

where  $i = 1, 2, \dots, N$  and  $M_i^x(k)$ ,  $M_i^\kappa(k)$ ,  $m_i(k)$ ,  $L_i^x(k)$ ,  $L_i^\kappa(k)$ ,  $l_i(k)$  are approximate dimension matrices; the detailed derivation process of these matrices is presented in [33]. In the two equations,  $\eta_i(k)$  and  $\gamma_i(k)$  are linear functions of  $\Delta x_i(k)$  and  $\kappa_i(k)$ , and the equilibrium equations are used as auxiliary equations to solve the game problem. The process of solving it is analytical and solutions can always be found. By using the recursive iteration method, the equilibrium strategy can be obtained as follows:

$$\begin{cases} \Delta\delta_{fi}(k) = K_{1i}^x(k)\Delta x_i(k) + K_{1i}^\kappa(k)\kappa_i(k) + \alpha_{1i}(k) \\ \Delta M_{zi}(k) = K_{2i}^x(k)\Delta x_i(k) + K_{2i}^\kappa(k)\kappa_i(k) + \alpha_{2i}(k) \end{cases} \quad (32)$$

where  $i = 0, 1, \dots, N - 1$ , and  $\Delta\delta_{fi}(k)$ ,  $\Delta M_{zi}(k)$  are, respectively, the additional front wheel steering angle and the additional yaw moment at stage  $i$ .  $K_{1i}^x(k)$ ,  $K_{2i}^x(k)$  and  $K_{1i}^\kappa(k)$ ,  $K_{2i}^\kappa(k)$  represent the gain arrays of error state and the Lagrange multiplier, respectively.  $\alpha_{1i}(k)$  and  $\alpha_{2i}(k)$  are the adjunctive terms of DYC and AFWS, respectively. All these gain arrays are the function of  $A_d$ ,  $B_{1d}$ ,  $B_{2d}$ ,  $S_1$ ,  $S_2$ ,  $Q_1$ ,  $Q_2$ ,  $R_1$  and  $R_2$ , so they do not change as time goes on. (Due to limited space, the detailed derivation process is neglected, but it can be found in [33] and [13].) It should be noted that only one stage game strategy can be applied to the control system at each time step, so only the first stage of game result is applied to the controller at each time step  $k$ , namely,  $\Delta\delta_{f0}(k)$ , and  $\Delta M_{z0}(k)$ .

### 3.3. LQR-Based Control Strategy

For proving the performance of the proposed Stackelberg game control algorithm, a discrete LQR controller is designed for comparison. In order to realize LQR based integration control strategy, the state space equation (Equation (14)) can be transformed into:

$$\Delta x(k + 1) = A_d\Delta x(k) + B\Delta u(k), \quad (33)$$

with

$$\begin{cases} B = \begin{bmatrix} B_{1d} & B_{2d} \end{bmatrix} \\ \Delta u(k) = \begin{bmatrix} \Delta\delta_f(k) & \Delta M_z(k) \end{bmatrix}^T \end{cases} \quad (34)$$

where  $B_{1d}$  and  $B_{2d}$  are the same as that presented in Equation (14). For the conventional discrete LQR control problem, the quadratic cost function can be constructed as follows:

$$J = \frac{1}{2} \sum_{k=0}^{\infty} [\Delta x^T(k) Q \Delta x(k) + \Delta u^T(k) R \Delta u(k)], \tag{35}$$

where  $Q$  and  $R$  are the real symmetric weight matrices with  $Q \geq 0, R > 0$ . The solution of the discrete LQR-based optimal control strategy can be presented as follows:

$$\Delta u(k) = -[R + B^T P B]^{-1} B^T P A_d \Delta x(k), \tag{36}$$

where  $P$  is the solution of the following algebraic Riccati equation and can be solved using the *dare* function in *Matlab*:

$$P = Q + A_d^T [P^{-1} + B R^{-1} B^T]^{-1} A_d. \tag{37}$$

It should be noted that the weight matrices in the LQR-based control strategy have the same definition as in the Stackelberg-based control strategy, as presented in Equations (19)–(22):

$$\begin{cases} Q = \text{diag} \begin{bmatrix} Q_\beta & Q_\omega \end{bmatrix} \\ R = \text{diag} \begin{bmatrix} R_\delta & R_{Mz} \end{bmatrix} \end{cases}. \tag{38}$$

#### 4. Lower-Level Controller

As shown in Figure 6, the objective vehicle is a FWID-EV. It is equipped with four in-wheel motors and by-wire steering motors as the terminal actuators. Thus, the virtual control commands,  $\Delta M_z$  and  $\Delta \delta_f$ , obtained in the upper-level controller should be further realized by the real actuators. In detail, the driving/braking torque  $T_i$  and steering angle  $\Delta \delta_i$  should be determined in the lower-level controller as shown in Figure 1; the subscripts  $i = 1, 2, 3, 4$  represent the front left, front right, rear left, and rear right tires, respectively (the same as in Figure 6). For simplicity, the steering angles of the same axle are assumed to be the same [34], namely,  $\delta_f = \delta_1 = \delta_2, \delta_r = \delta_3 = \delta_4$ .

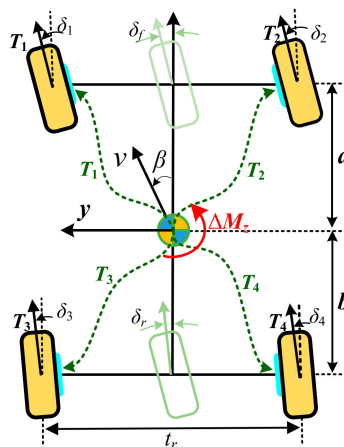


Figure 6. Allocation of virtual control variables.

For the AFWS, the additional rear wheel steering angle can be obtained according to Equation (5):

$$\Delta \delta_r = \iota \cdot \Delta \delta_f. \tag{39}$$

Therefore, the additional steering control command,  $\Delta \delta_f$  and  $\Delta \delta_r$ , can be directly distributed to the steering motors and performed with by-wire technology.

For the DYC, the additional yaw moment  $\Delta M_z$  can be obtained by distributing different driving/braking torque to the four wheels, which can be treated as a constrained optimization

problem. The tire utilization rate is an important index to judge the degree of vehicle stability [35], so the optimization problem can be formulated as follows:

$$\begin{aligned} \min f(F_x) &= \frac{F_{x1}^2 + F_{y1}^2}{\mu^2 F_{z1}^2} + \frac{F_{x2}^2 + F_{y2}^2}{\mu^2 F_{z2}^2} + \frac{F_{x3}^2 + F_{y3}^2}{\mu^2 F_{z3}^2} + \frac{F_{x4}^2 + F_{y4}^2}{\mu^2 F_{z4}^2} \\ \text{s.t.} \left\{ \begin{aligned} U_1(F_x) &: \Delta M_z - \left[ t_r/2(F_{x2} - F_{x1}) \cos \delta_f + a(F_{x1} + F_{x2}) \sin \delta_f \right. \\ &\quad \left. + t_r/2(F_{x4} - F_{x3}) \cos \delta_r - b(F_{x3} + F_{x4}) \sin \delta_r \right] = 0 \\ U_2(F_x) &: F_{x1} + F_{x2} + F_{x3} + F_{x4} - F_s = 0 \\ W_i(F_x) &: |F_{xi}| - (T_{max}/r) \leq 0, i = 1, 2, 3, 4 \\ Z_i(F_x) &: F_{xi}^2 + F_{yi}^2 - (\mu^{F_{zi}})^2 \leq 0, i = 1, 2, 3, 4 \end{aligned} \right. \end{aligned} \tag{40}$$

where  $F_x = [F_{x1}, F_{x2}, F_{x3}, F_{x4}]^T$  and represents the corresponding longitudinal tire forces.  $\mu$  is the road adhesion coefficient.  $F_{zi}$  and  $F_{yi}$  are the vertical and lateral forces of the tire  $i$ , respectively. It is assumed that road adhesion coefficient and tire forces in the vertical and lateral direction can be estimated [36].  $\delta_f$  and  $\delta_r$  are the actual front and rear wheels steering angle, respectively.  $r$  is the tire effective rolling radius;  $t_r$  is the wheel track.  $T_{max}$  is the maximum output torque of the in-wheel motor.  $F_s$  is the sum of the four wheels' tire longitudinal force. In order to reduce the influence of DYC on the vehicle longitudinal dynamic,  $F_s$  is set to 0.

For avoiding the interference of the active steering angle of Equation (39) with the longitudinal tire force optimization of Equation (40), the actual front and rear wheel steering angles,  $\delta_f$  and  $\delta_r$ , in constraint conditions of the optimization problem in Equation (40), are set as follows:

$$\begin{cases} \delta_f = \delta_{fd} + \Delta\delta_f \\ \delta_r = \delta_{rd} + \Delta\delta_r \end{cases} \tag{41}$$

where  $\delta_f$  and  $\delta_r$  represent the total steering angles applied to the front and rear wheels, respectively. Then, the optimization problem in Equation (40) can be regarded as a pure DYC problem [37] and the virtual signal  $\Delta M_z$  in the upper-level controller can be accurately realized.

Equation (40) is a small nonlinear optimization problem with multiple constraints. Sequential quadratic programming (SQP) is a powerful and effective method for solving this kind of nonlinear optimization problem [38]. Moreover, the convergence of the SQP algorithm can be guaranteed due to the definite nature of the approximate Hessian matrix of the constructed Lagrangian function [39], and the uniqueness of the solution can ensure that a global minimum is found [40]. Therefore, the SQP method is used to realize the control commands,  $\Delta M_z$ , in DYC by solving the optimization problem in Equation (40).

The main principle of SQP is to solve the nonlinear optimization problem by linearizing the system [39]. The Lagrangian function is constructed for solving the SQP problem:

$$L(F_x, \alpha_i, \beta_i, \xi_i) = f(F_x) + \sum_{i=1}^2 \alpha_i U_i(F_x) + \sum_{i=1}^4 \beta_i W_i(F_x) + \sum_{i=1}^4 \xi_i Z_i(F_x), \tag{42}$$

where  $\alpha_i$ ,  $\beta_i$ , and  $\xi_i$  are the Lagrange multipliers. At each iteration of SQP, the current approximate Hessian matrix of Lagrange function  $H_n$  in Equation (43) is constructed. Then, the nonlinear optimization problem is transformed into a series of quadratic programming (QP) subproblems:

$$\begin{aligned} \min & \nabla f(F_{xn})^T d_n + \frac{1}{2} d_n^T H_n d_n \\ \text{s.t.} \left\{ \begin{aligned} U_i(F_{xn}) + \nabla U_i(F_{xn}) d_n &= 0, i = 1, 2 \\ W_i(F_{xn}) + \nabla W_i(F_{xn}) d_n &\leq 0, i = 1, 2, 3, 4 \\ Z_i(F_{xn}) + \nabla Z_i(F_{xn}) d_n &\leq 0, i = 1, 2, 3, 4 \end{aligned} \right. \end{aligned} \tag{43}$$

where  $\nabla$  denotes the gradient;  $d_n$  and  $F_{xn}$  are the search direction and the tire longitudinal force at iteration step  $n$ , respectively.  $H_n$  is updated by the Broyden-Fletcher-Goldfarb-Shanno (BFGS) method [39]. The quadratic programming sub-problem in Equation (43) is solved by the mature QP algorithm in [39]. The search direction  $d_n$  is concluded by solving the QP subproblem in Equation (43), which is used to generate a new iteration  $F_{x(n+1)}$ :

$$F_{x(n+1)} = F_{xn} + \zeta_n d_n, \quad (44)$$

where  $\zeta_n$  is the step length parameter, which is determined by a line search procedure.

The steps for solving the SQP problem can be summarized in the following process (Algorithm 1):

---

**Algorithm 1:** Iteration process of SQP Algorithm

---

- 1: Initializing  $F_{xn}$  and Hessian matrix  $H_n$ .
- 2: Defining  $\rho > 0$ ,  $v > 0$ ,  $n = 0$ .
- 3: Solving  $d_n$  in the QP sub-problem in (43).
  - If  $|d_n| \leq \rho$ , then break;
  - If  $|d_n| > \rho$ , continue;
- 4: Calculating the step length parameter  $\zeta_n$  that can make a decrease of merit function  $l(F_{xn})$  [38,41].

$$\zeta_n = \arg \min_{0 \leq \zeta \leq v} l(F_{xn} + \zeta_n d_n) \quad (45)$$

$$l(F_{xn}) = f(F_{xn}) + \sum_{i=1}^2 a_i \cdot U_i(F_{xn}) + \sum_{i=1}^4 b_i \cdot W_i(F_{xn}) + \sum_{i=1}^4 c_i \cdot Z_i(F_{xn}), \quad (46)$$

where

$$\begin{cases} a_i = \max\left\{\alpha_i, \frac{\alpha_i + \alpha_i}{2}\right\}, i = 1, 2. \\ b_i = \max\left\{\beta_i, \frac{\beta_i + \beta_i}{2}\right\}, i = 1, 2, 3, 4. \\ c_i = \max\left\{\xi_i, \frac{\xi_i + \xi_i}{2}\right\}, i = 1, 2, 3, 4 \end{cases} \quad (47)$$

$a_i, b_i, c_i$  are initialized by

$$\begin{cases} a_i = \frac{\|\nabla f(F_{xn})\|}{\|\nabla U_i(F_{xn})\|}, i = 1, 2. \\ b_i = \frac{\|\nabla f(F_{xn})\|}{\|\nabla W_i(F_{xn})\|}, i = 1, 2, 3, 4 \\ c_i = \frac{\|\nabla f(F_{xn})\|}{\|\nabla Z_i(F_{xn})\|}, i = 1, 2, 3, 4 \end{cases} \quad (48)$$

- 5: Calculating the next step value of  $F_{x(n+1)}$ :

$$F_{x(n+1)} = F_{xn} + \zeta_n d_n \quad (49)$$

- 6: Updating the Hessian matrix  $H_{n+1}$  by using the BFGS [39] method:

$$H_{n+1} = H_n - \frac{H_n s_n s_n^T H_n}{s_n^T H_n s_n} + \frac{z_n z_n^T}{s_n^T z_n}, \quad (50)$$

there exists

$$\begin{cases} z_n = \theta_n y_n + (1 - \theta_n) H_n s_n \\ s_n = F_{x(n+1)} - F_{xn} \\ y_n = \nabla_{F_{x(n+1)}} L(F_{x(n+1)}, \alpha_i, \beta_i) - \nabla_{F_{xn}} L(F_{xn}, \alpha_i, \beta_i) \end{cases}, \quad (51)$$

where  $\theta_n$  is defined as follows:

$$\theta_n = \begin{cases} \frac{0.8 s_n^T H_n s_n}{s_n^T H_n s_n - s_n^T y_n}, & s_n^T y_n < 0.2 s_n^T H_n s_n \\ 1, & s_n^T y_n \geq 0.2 s_n^T H_n s_n \end{cases} \quad (52)$$

- 7: Setting  $n = n + 1$ ; then return to step 3 and continue.
-

For getting the distributed tire longitudinal forces, the driving/braking torque of motors are found as follows:

$$T_x = \frac{1}{1 + \tau_x s} F_x \cdot r, \quad (53)$$

where  $T_x = [T_{x1}, T_{x2}, T_{x3}, T_{x4}]^T$  and  $T_{xi}$  with  $i = 1, 2, 3, 4$  representing the driving/braking torque of the corresponding wheels.  $\tau_x$  represents the motor's delay time.  $r$  is the tire effective rolling radius. Compared with the electromagnetic dynamics of the motor, the mechanical motion of the vehicle is much slower [42], so we assume that the motor driver and the in-wheel motor's dynamic responses are ignored.

## 5. Simulation Results

The proposed control strategy is evaluated by the cosimulation of *CarSim* and *Matlab/Simulink*. The commercial software *CarSim* provides a full-vehicle dynamic model and the proposed controller is constructed in *Matlab/Simulink*. Two different test maneuvers are used in this paper. The first maneuver is the open-loop sinusoidal steering angle input test, which is an effective method for testing vehicles' handling performance [43]. The second is a closed-loop double lane change (DLC) maneuver with the driver in the loop. In these simulations, a low road adhesion coefficient ( $\mu = 0.6$ ) with a 100 km/h initial velocity is implemented to test the proposed controller's performance. The B-class sports car provided by *CarSim* is used as the simulation model. For guaranteeing the characteristics of the original car, the parameters used in this paper, which are shown in Table 1, come from that car.

**Table 1.** Key parameters of vehicle model.

Variable	Parameter Name	Units	Value
$m$	Vehicle mass	kg	1140
$k_f$	Cornering stiffness of front tires	N/rad	82,000
$k_r$	Cornering stiffness of rear tires	N/rad	130,000
$a$	Distance from CG to front axle	m	1.165
$b$	Distance from CG to rear axle	m	1.165
$r$	Radius of wheel	m	0.31
$R_{st}$	Steering gear ratio	/	14.5
$I_z$	Yaw moment of inertia	kg/m <sup>2</sup>	996
$t$	Track distance	m	1.481
$h$	Height of CG	m	0.375
$T_{max}$	Peak torque of motor	N.m	500

The weighting matrices of the proposed Stackelberg and LQR controller in the upper level are chosen as follows:

$$Q = S_1 = S_2 = Q_1 = Q_2 = \begin{bmatrix} 30 & 0 \\ 0 & 60 \end{bmatrix}. \quad (54)$$

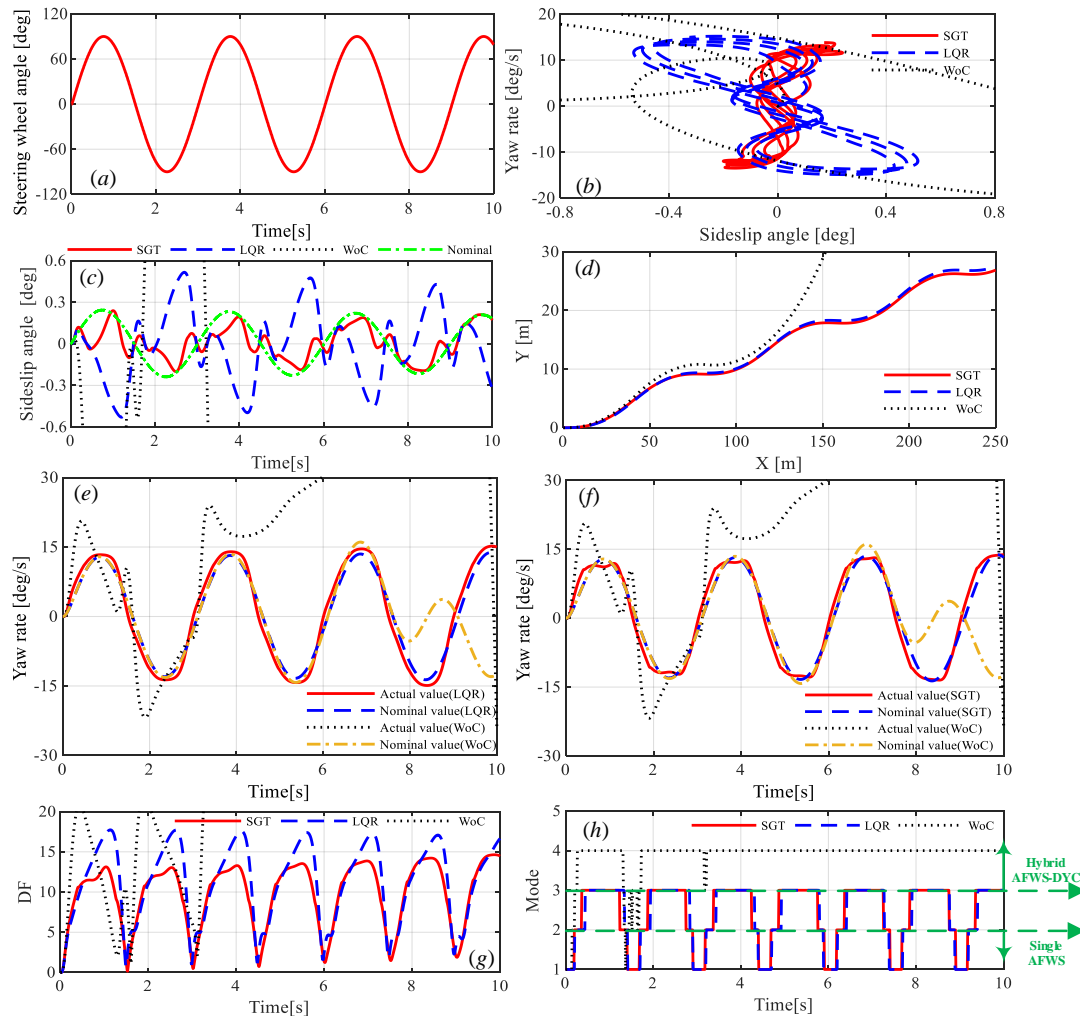
The game stage  $N$  is set to 50, while the other controller parameters, such as  $T_s$ ,  $p$ ,  $q$ ,  $R_\delta$  and  $R_{Mz}$ , have been defined in Equations (15), (16), (20)–(22), respectively. These weight coefficients are selected by iterative tuning in simulation tests. Meanwhile, the controller parameters in the lower-level controller are defined as follows:

$$\rho = 10^{-8}, v = 1, \tau_x = 0.01. \quad (55)$$

The time step of the simulation is selected as 0.01 s. The above values, including all controller parameters and other related values, can be calculated by the corresponding equations provided in this paper. Simulation results and analysis are given in the next two sections.

### 5.1. Open-Loop Sinusoidal Input Test

In the open-loop sinusoidal input test, the steering wheel angle's input is a sine wave with an amplitude of  $90^\circ$  and a frequency of  $1/3$  Hz, as shown in Figure 7a. For ease of expression, the abbreviations SGT and LQR in the following figures denote control based on the Stackelberg game theory and the LQR method, respectively. WoC means a response without control.



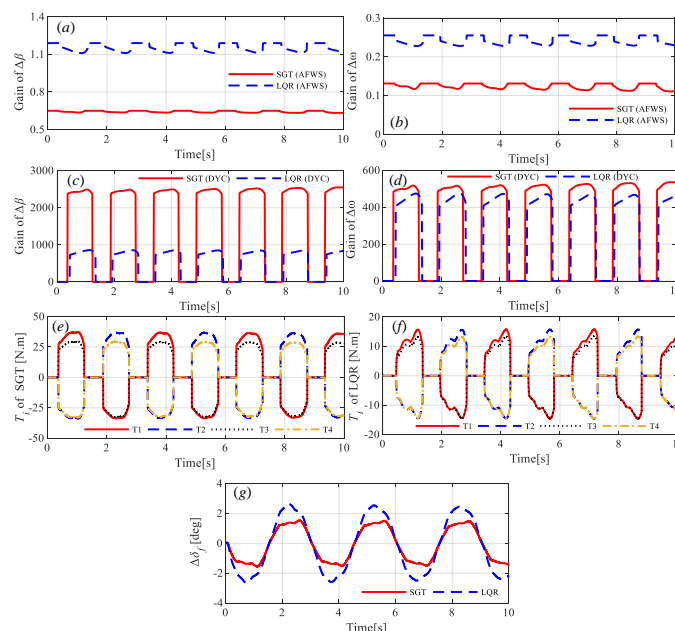
**Figure 7.** Steering input and dynamic responses of open-loop sinusoidal steering test at 100 km/h. (a) Sinusoidal steering wheel angle; (b)  $\beta$ - $\omega$  phase portraits; (c) sideslip angle; (d) Y position; (e) yaw rate of LQR; (f) yaw rate of SGT; (g) dangerous factor (DF); (h) working mode.

Figure 7b–f shows the  $\beta$ - $\omega$  phase portraits, sideslip angle, vehicle position, and yaw rate responses, respectively, under different control strategies. It can be seen that the vehicle without control has lost stability at about 4 s. As shown in Figure 7b,c, the vehicle with a SGT controller can maintain the phase portraits in a smaller envelope and keep the amplitude of the sideslip angle in a smaller range compared with that with a LQR-based controller. In addition, it can be seen from Figure 7e,f that the SGT vehicle can track the nominal yaw rate better and better as time goes on, while the deviation between the actual and nominal values of LQR vehicle becomes larger later on in the testing, so the proposed SGT algorithm can return the vehicle to a better state.

Figure 7g,h shows the vehicle's DF index and working mode, respectively. It can be seen from Figure 7g that the DF values controlled by LQR are larger than those controlled by SGT because of the bad state responses of the vehicle with LQR. In Figure 7h, the numbers 1, 2, 3, 4 represent the working regions I, II, III, IV respectively, of Figure 3. It can be seen that the vehicle with LQR and SGT works in

a similar mode, while the vehicle WoC spent most of its time in mode 4, which means it exhibited a poor condition for a longer time. The results indicated that the SGT-based controller could stabilize the vehicle in a safe dynamic state and reduce the possibility of losing lateral stability compared with the LQR.

Figure 8 presents the vehicle state gain array and controller output, respectively. Figure 8a–d shows the AFWS and DYC controllers' gains of vehicle states ( $\Delta x$ ) resulting from the game theory (SGT)-based approach, i.e., the gains in Equation (32), compared with those resulting from the LQR approach, i.e., the gain of  $\Delta x$  in Equation (36). The state gains of the AFWS controller are shown in Figure 8a,b and those of the DYC controller are shown in Figure 8c,d. It can be seen that the LQR controller generates a larger gain with AFWS control, whilst SGT yields a higher gain with DYC due to the larger control authority of the leader (DYC) in the Stackelberg game process. Moreover, the gain fluctuates with the change in DF, as shown in Figure 7g. It can be seen that as the DF increases, the gain of AFWS has a declining trend, while the gain of DYC appears to have an opposite trend and becomes 0 when the vehicle stays in mode 1 or 2, as shown in Figure 7h. The results demonstrated that the proposed adaptive weight-adjusting mechanism (AWAW) corresponding to the double-mode control strategy works well, as described in an upper-level controller and shown in Equations (20)–(22).



**Figure 8.** State gains and control inputs of open-loop sinusoidal steering test at 100 km/h. (a) Gain of  $\Delta\beta$  (AFWS); (b) gain of  $\Delta\omega$  (AFWS); (c) gain of  $\Delta\beta$  (DYC); (d) gain of  $\Delta\omega$  (DYC); (e) additional torque of SGT; (f) additional torque of LQR; (g) additional front wheel steering angle.

The control outputs of DYC and AFWS are shown in Figure 8e–g, which is a reflection of the state gains in Figure 8a–d. As shown in Figure 8e,f, the driving/braking torques with SGT are almost twice as high as with LQR, while the additional steering angle with SGT is smaller than that with LQR, as shown in Figure 8g. The results demonstrated that more control authority is allocated to DYC compared with AFWS under the SGT-based controller. It should be noted that the control authority of the two players is determined by the game. In the framework of the Stackelberg game, the leader (DYC) acts first to stabilize the vehicle based on the working region, then the follower (AFWS) just makes an optimal response to the action of the leader to ensure the vehicle stability. All these results demonstrate that cooperative control with SGT can better help a driver to stabilize a vehicle under a severe maneuver, whereas LQR only treats the control of the two systems as an optimal problem without considering the interaction between them. The additional steering angles of AFWS in the rear

wheel with SGT and LQR are similar to the controlled angles in the front wheel, but with a difference in the amplitude according to Equation (5), so they are not presented here.

### 5.2. Closed-Loop Double-Lane-Change Test

To verify the effectiveness of the proposed control strategy under disturbance, a closed-loop double-lane-change (DLC) maneuver is performed with a driver in the loop. A built-in driver model of *CarSim* is used to make the steering decision. For highlighting the performance, the driver's preview time is set as 0.65 s to trigger an unstable case.

Figure 9 shows the vehicle dynamic responses with a driver in the loop under different control strategies. As shown in Figure 9a, the sideslip angle with SGT is much smaller than that with LQR; the maximum peak value was reduced by 62.4% compared to that of LQR. Meanwhile, the sideslip angle with WoC becomes very large at the beginning of DLC, which implies that the vehicle without control has lost stability during this severe maneuver. Figure 9b shows the phase trajectory of the side slip angle and yaw rate. It is clear that the area covered by the phase trajectory with SGT is much smaller than that with LQR.

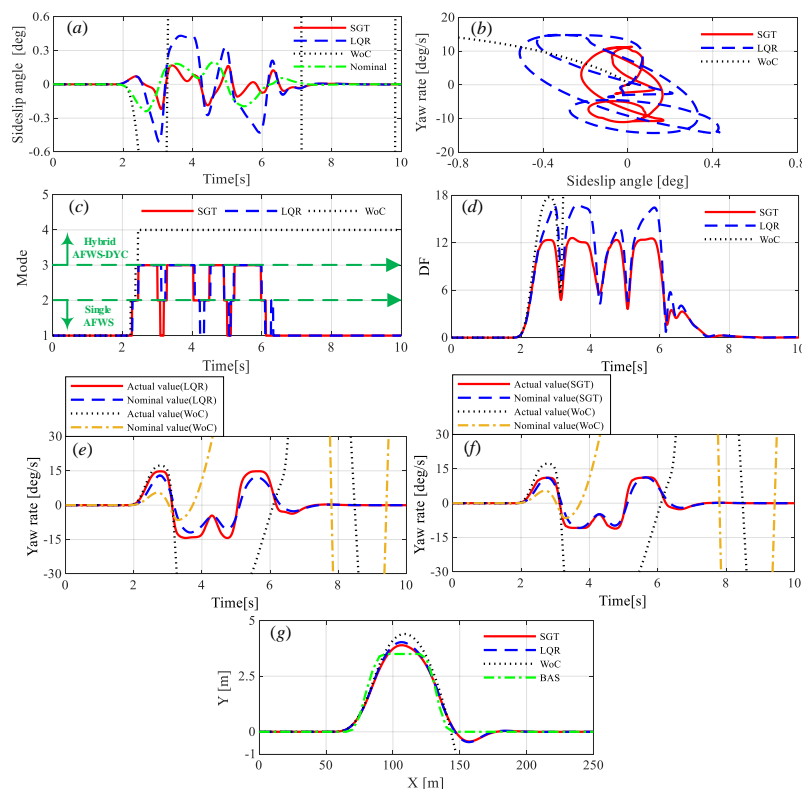


**Figure 9.** Dynamic responses of DLC test at 100 km/h. (a) Sideslip angle; (b)  $\beta$ - $\omega$  phase portraits; (c) working mode; (d) dangerous factor (DF); (e) yaw rate of LQR; (f) yaw rate of SGT; (g) Y position.

Figure 9c,d presents the working mode and DF index, respectively. It can be seen that in most DLC maneuvers the vehicle works in region III or II for both SGT and LQR, as shown in Figure 9c, but spends relatively more time in region II with SGT. Also, as shown in Figure 9d, the DF index of SGT is much smaller than that of LQR for the same case. This means that a vehicle with SGT behavior is more stable compared to the case with LQR. Figure 9e,f shows the yaw rate under LQR and SGT, respectively, by comparing it to their nominal value. It is clear that the yaw rate response with SGT is smaller than that with LQR. Also, the tracking performance for the nominal yaw rate is much better by the SGT. However, for the case without control, the yaw rate runs out of the nominal region, and the vehicle becomes unstable even with a driver in the loop. Figure 9g shows the vehicle trajectories and

BAS denotes the desired trajectory as a normal DLC. In this process, a vehicle with SGT can track the desired trajectory more precisely than with LQR, and a vehicle without control finally deviates from the desired trajectory. All the results demonstrated that a vehicle with SGT has better dynamic responses than with LQR in terms of both lateral stability and path tracking performance, whereas a vehicle without control soon loses dynamic stability during a severe DLC maneuver. This conclusion is consistent with that of the sine test.

Figure 10a–d show the state gains of AFWS and DYC under SGT and LQR, respectively. The variation in these adaptive gains is similar to what appears in the sinusoidal test case, especially when the vehicle performs a steering maneuver. As defined in Equations (21) and (22), the weight coefficients of the controller outputs change as DF varies, which causes a change in gains only when working in hybrid mode. Similarly, the gains of AFWS with SGT are smaller than those with LQR. In other words, for the same case, SGT allocates more control authority to DYC based on the idea of a leader-follower game.

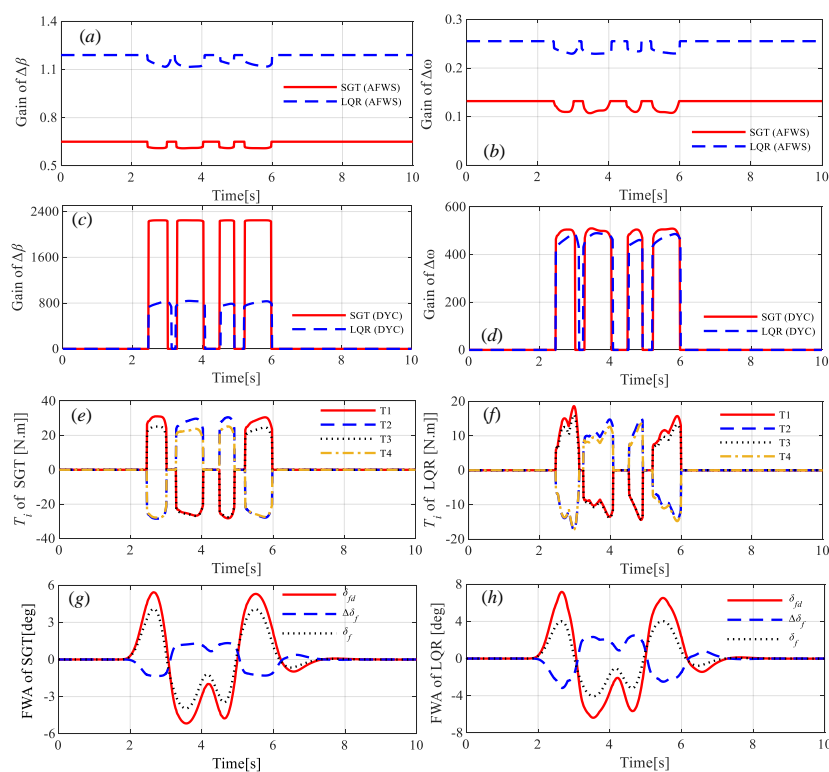


**Figure 10.** State gains and control inputs of DLC test at 100 km/h. (a) Gain of  $\Delta\beta$  (AFWS); (b) Gain of  $\Delta\omega$  (AFWS); (c) gain of  $\Delta\beta$  (DYC); (d) gain of  $\Delta\omega$  (DYC); (e) additional torque of SGT; (f) additional torque of LQR; (g) front wheel angle (FWA) of SGT; (h) front wheel angle (FWA) of LQR.

Figure 10e–h presents the control actions of DYC and AFWS. The variation of motor torque and steering angle are closely related to the state gains in Figure 10a–d. As shown in Figure 10e,f, the additional driving/braking torque of SGT is almost twice as much as that of LQR, because the gains of DYC in the SGT vehicle are larger than those of the LQR-based vehicle, as shown in Figure 10c,d. In Figure 10g,h,  $\delta_{fd}$  is the steering angle produced by the driver in the front wheel,  $\Delta\delta_f$  is the additional steering angle of AFWS, and  $\delta_f$  is the total steering angle performed by the steering motor. The additional steering angle of AFWS with SGT is almost half that with LQR. The results implied that less control authority is allocated to the AFWS when working with SGT compared to that with LQR, which is consistent with the conclusions of the sine test.

## 6. Conclusions

This paper presents a leader-follower game-based cooperative control strategy for the stability control of a special FWID-EV. The two subsystems, AFWS and DYC, are regarded as the two players in the Stackelberg game model. A hierarchical control strategy is designed to guarantee the lateral stability of FWID-EV under severe conditions. In this strategy, the Stackelberg game controller can properly adjust the control authority between AFWS and DYC, while the SQP method could realize the virtual additional yaw moment highly efficiently by allocating the driving/braking torque to the four wheels. A cosimulation with CarSim and Matlab/Simulink is performed to verify the effectiveness of the proposed algorithm. The results demonstrate that the proposed Stackelberg game controller can improve the vehicle's lateral stability and path-following compared to a LQR-based stability controller.

**Author Contributions:** L.Z. and S.L. conceived the original ideas; L.Z. and B.Z. performed the simulations; S.L. directed the overall project; S.L. and L.Z. analyzed the data. L.Z. and S.L. wrote the manuscript. All authors discussed the results.

**Funding:** This research was funded by the National Natural Science Foundation of China (51675066, 51005256), Chongqing Research Program of Basic Research and Frontier Technology (cstc2017jcyjAX0323), and Fundamental Research Funds for the Central Universities (2019CDXYQC0002).

**Acknowledgments:** The authors would also like to thank the reviewers for their corrections and helpful suggestions.

**Conflicts of Interest:** The authors declare no conflict of interest.

## References

- Hu, C.; Wang, R.; Yan, F. Integral Sliding Mode-Based Composite Nonlinear Feedback Control for Path Following of Four-Wheel Independently Actuated Autonomous Vehicles. *IEEE Trans. Transp. Electr.* **2016**, *2*, 221–230. [[CrossRef](#)]
- Cao, W.; Liu, H.; Lin, C.; Chang, Y.; Liu, Z.; Szumanowski, A. Co-Design Based Lateral Motion Control of All-Wheel-Independent-Drive Electric Vehicles with Network Congestion. *Energies* **2017**, *10*, 1641. [[CrossRef](#)]
- Hori, Y. Future vehicle driven by electricity and Control-research on four-wheel-motored "UOT electric march II". *IEEE Trans. Ind. Electron.* **2004**, *51*, 954–962. [[CrossRef](#)]
- Wu, J.; Cheng, S.; Liu, B.; Liu, C.; Sciubba, E. A Human-Machine-Cooperative-Driving Controller Based on AFS and DYC for Vehicle Dynamic Stability. *Energies* **2017**, *10*, 1737. [[CrossRef](#)]
- Wang, Z.; Zhu, J.; Zhang, L.; Wang, Y. Automotive ABS/DYC Coordinated Control under Complex Driving Conditions. *IEEE Access* **2018**, *6*, 32769–32779. [[CrossRef](#)]
- Zhu, B.; Chen, Y.; Zhao, J. Integrated chassis control of active front steering and yaw stability control based on improved inverse nyquist array method. *Sci. World J.* **2014**, *2014*, 919847. [[CrossRef](#)] [[PubMed](#)]
- Jin, X.; Yu, Z.; Yin, G.; Wang, J. Improving Vehicle Handling Stability Based on Combined AFS and DYC System via Robust Takagi-Sugeno Fuzzy Control. *IEEE Trans. Intell. Transp. Syst.* **2018**, *19*, 2696–2707. [[CrossRef](#)]
- Peng, J.; He, H.; Feng, N. Simulation Research on an Electric Vehicle Chassis System Based on a Collaborative Control System. *Energies* **2013**, *6*, 312–328. [[CrossRef](#)]
- Mokhiamar, O.; Abe, M. Simultaneous optimal distribution of lateral and longitudinal tire forces for the model following control. *J. Dyn. Syst. Meas. Control* **2004**, *126*, 753–763. [[CrossRef](#)]
- Tamaddoni, S.H.; Taheri, S.; Ahmadian, M. Optimal preview game theory approach to vehicle stability controller design. *Veh. Syst. Dyn.* **2011**, *49*, 1967–1979. [[CrossRef](#)]
- Cruz, J., Jr. Survey of nash and stackelberg equilibrium strategies in dynamic games. In *Annals of Economic and Social Measurement*; Berg, S.V., Ed.; NBER: Cambridge, MA, USA, 1975; Volume 4, pp. 339–344.
- Başar, T.; Olsder, G.J. *Dynamic Noncooperative Game Theory*, 2nd ed.; Academic Press: New York, NY, USA, 1995; pp. 365–421.
- Na, X.; Cole, D.J. *Modelling Driver-AFS Interactive Steering Control Using the Principle of Open-Loop Stackelberg Equilibrium*; CUED/TR. 101; Department of Engineering, University of Cambridge: Cambridge, UK, 2013.
- Na, X.; Cole, D.J. Game-Theoretic Modeling of the Steering Interaction between a Human Driver and a Vehicle Collision Avoidance Controller. *IEEE Trans. Hum. Mach. Syst.* **2015**, *45*, 25–38. [[CrossRef](#)]

15. Myerson, R.B. *Game Theory: Analysis of Conflict*; Harvard University Press: Cambridge, MA, USA, 1991; pp. 1–33.
16. Tamaddoni, S.H.; Taheri, S.; Ahmadian, M. Optimal VSC design based on Nash strategy for differential 2-player games. In Proceedings of the IEEE International Conference on Systems, Man and Cybernetics, San Antonio, TX, USA, 11–14 October 2009.
17. Tamaddoni, S.H.; Taheri, S.; Ahmadian, M. Optimal Direct Yaw Controller Design for Vehicle Systems with Human Driver. *SAE Int. J. Commer. Veh.* **2011**, *4*, 13–21. [[CrossRef](#)]
18. Na, X.; Cole, D.J. Linear quadratic game and non-cooperative predictive methods for potential application to modelling driver-AFS interactive steering control. *Veh. Syst. Dyn.* **2012**, *51*, 165–198. [[CrossRef](#)]
19. Ji, X.; Liu, Y.; Na, X.; Liu, Y. Research on interactive steering control strategy between driver and AFS in different game equilibrium strategies and information patterns. *Veh. Syst. Dyn.* **2018**, *56*, 1344–1374. [[CrossRef](#)]
20. Jie, Z.; Zhang, Y. Fractional-order PI $\lambda$ D $\mu$  control and optimization for vehicle active steering. In Proceedings of the 7th World Congress on Intelligent Control and Automation, Chongqing, China, 25 June 2008.
21. Na, X.; Cole, D.J. Application of Open-Loop Stackelberg Equilibrium to Modeling a Driver's Interaction with Vehicle Active Steering Control in Obstacle Avoidance. *IEEE Trans. Hum. Mach. Syst.* **2017**, *47*, 673–685. [[CrossRef](#)]
22. Nagai, M.; Hirano, Y.; Yamanaka, S. Integrated Robust Control of Active Rear Wheel Steering and Direct Yaw Moment Control. *Veh. Syst. Dyn.* **2007**, *29*, 416–421. [[CrossRef](#)]
23. Rajamani, R. *Vehicle Dynamics and Control*; Springer Science Business: New York, NY, USA, 2006; pp. 221–255.
24. Sano, S. Four wheel steering system with rear wheel steer angle controlled as a function of steering wheel angle. *SAE Trans.* **1986**, *95*, 880–893.
25. Yang, X.; Wang, Z.; Peng, W. Coordinated control of AFS and DYC for vehicle handling and stability based on optimal guaranteed cost theory. *Veh. Syst. Dyn.* **2008**, *47*, 57–79. [[CrossRef](#)]
26. Nagai, M.; Shino, M.; Gao, F. Study on integrated control of active front steer angle and direct yaw moment. *JSAE Rev.* **2002**, *23*, 309–315. [[CrossRef](#)]
27. Beal, C.E.; Bobier, C.G.; Gerdes, J.C. Controlling vehicle instability through stable handling envelopes. In Proceedings of the ASME 2011 Dynamic Systems and Control Conference and Bath/ASME Symposium on Fluid Power and Motion Control, Arlington, VA, USA, 1 January 2011.
28. Cheng, S.; Li, L.; Mei, M.M.; Nie, Y.L.; Zhao, L. Multiple-Objective Adaptive Cruise Control System Integrated with DYC. *IEEE Trans. Veh. Technol.* **2019**, *68*, 4550–4559. [[CrossRef](#)]
29. Manning, W.; Selby, M.; Crolla, D.; Brown, M. IVMC: Intelligent Vehicle Motion Control. In Proceedings of the SAE International, SAE Technical Paper 2002-01-0821, Detroit, MI, USA, 4–7 March 2002.
30. Wang, J.; Longoria, R.G. Coordinated and Reconfigurable Vehicle Dynamics Control. *IEEE Trans. Control Syst. Technol.* **2009**, *17*, 723–732. [[CrossRef](#)]
31. Li, M.; Cruz, J.; Simaan, M.A. An approach to discrete-time incentive feedback Stackelberg games. *IEEE Trans. Syst. Man. Cybern. A Syst. Hum.* **2002**, *32*, 472–481.
32. Lewis, F.L.; Vrabie, D.L.; Syrmos, V.L. *Optimal Control*, 3rd ed.; John Wiley & Sons: Hoboken, NJ, USA, 2015; pp. 19–102.
33. Hungerländer, P.; Neck, R. An Algorithmic Equilibrium Solution for N-Person Dynamic Stackelberg Difference Games with Open-Loop Information Pattern. In *Computational Methods in Economic Dynamics*; Springer: Berlin, Germany, 2011; pp. 197–214.
34. Wang, J.; Longoria, R.G. Coordinated vehicle dynamics control with control distribution. In Proceedings of the 2006 American Control Conference, Minneapolis, MN, USA, 14–16 June 2006.
35. Lu, S.; Cen, S.; Zhang, Y. Driver Model-Based Fault-Tolerant Control of Independent Driving Electric Vehicle Suffering Steering Failure. *Autom. Innov.* **2018**, *1*, 85–94. [[CrossRef](#)]
36. Hsiao, T.; Lan, J.; Yang, H. Integrated estimation of vehicle states, tire forces, and tire-road friction coefficients. In Proceedings of the 14th International Conference on Control, Automation and Systems (ICCAS), Seoul, Korea, 22–25 October 2014.
37. Ding, N.; Taheri, S. An adaptive integrated algorithm for active front steering and direct yaw moment control based on direct Lyapunov method. *Veh. Syst. Dyn.* **2010**, *48*, 1193–1213. [[CrossRef](#)]

38. Yi, L.; Jinwu, X. Optimization of range and endurance of a propeller UAV based on SQP algorithm. In Proceedings of the IEEE International Conference on Unmanned Systems (ICUS), Beijing, China, 27–29 October 2017.
39. Nocedal, J.; Wright, S.J. *Numerical Optimization*; Springer Science Business: New York, NY, USA, 2006; pp. 529–561.
40. Padilla, G.P.; Weiland, S.; Donkers, M.C.F. A Global Optimal Solution to the Eco-Driving Problem. *IEEE Control Syst. Lett.* **2018**, *2*, 599–604. [[CrossRef](#)]
41. Morshed, M.J.; Asgharpour, A. Hybrid imperialist competitive-sequential quadratic programming (HIC-SQP) algorithm for solving economic load dispatch with incorporating stochastic wind power: A comparative study on heuristic optimization techniques. *Energy Convers. Manag.* **2014**, *84*, 30–40. [[CrossRef](#)]
42. Wang, R.; Wang, J. Fault-Tolerant Control with Active Fault Diagnosis for Four-Wheel Independently Driven Electric Ground Vehicles. *IEEE Trans. Veh. Technol.* **2011**, *60*, 4276–4287. [[CrossRef](#)]
43. Jin, L.; Gao, L.; Jiang, Y.; Chen, M.; Zheng, Y.; Li, K. Research on the control and coordination of four-wheel independent driving/steering electric vehicle. *Adv. Mech. Eng.* **2017**, *9*, 1–13. [[CrossRef](#)]



© 2019 by the authors. Licensee MDPI, Basel, Switzerland. This article is an open access article distributed under the terms and conditions of the Creative Commons Attribution (CC BY) license (<http://creativecommons.org/licenses/by/4.0/>).